

# Deep Discriminative to Kernel Generative Networks for Calibrated Inference

Jayanta Dey,<sup>1,\*</sup> Haoyin Xu,<sup>1</sup> Ashwin De Silva,<sup>1</sup> Will LeVine,<sup>1,2</sup> Tyler M. Tomita,<sup>1</sup> Ali Geisa,<sup>1</sup> Tiffany Chu,<sup>1</sup> Jacob Desman,<sup>1</sup> and Joshua T. Vogelstein<sup>1</sup>

**Abstract.** The fight between discriminative versus generative goes deep, in both the study of artificial and natural intelligence. In our view, both camps have complementary values. So, we sought to synergistically combine them. Here, we propose a methodology to convert deep discriminative networks to kernel generative networks. We leveraged the fact that deep models, including both random forests and deep networks, learn internal representations which are unions of polytopes with affine activation functions to conceptualize them both as generalized partitioning rules. We replace the affine function in each polytope populated by the training data with Gaussian kernel that results in a generative model. Theoretically, we derive the conditions under which our generative models are a consistent estimator of the corresponding class conditional density. Moreover, our proposed models obtain well calibrated posteriors for in-distribution, and extrapolate beyond the training data to handle out-of-distribution inputs reasonably. We believe this approach may be an important step in unifying the thinking and the approaches across the discriminative and the generative divide.

**1 Introduction** Machine learning methods, specially deep neural networks and random forests have shown excellent performance in many real-world tasks, including drug discovery, autonomous driving and clinical surgery. However, calibrating confidence over the whole feature space for these models remains a key challenge in the field. Although these learning algorithms can achieve near optimal performance at inferring on the samples lying in the high density regions of the training data [1–3], they yield highly confident predictions for the samples lying far away from the training data [4]. Calibrated confidence within the training or in-distribution (ID) region as well as in the out-of-distribution (OOD) region is crucial for safety critical applications like autonomous driving and computer-assisted surgery, where any aberrant reading should be detected and taken care of immediately [4, 5]. A well-calibrated model capable of quantifying the uncertainty associated with inference for any points from the training distribution as well as detecting OOD data can be a life-saver in these cases.

The approaches to calibrate OOD confidence for learning algorithms described in the literature can be roughly divided into two groups: discriminative and generative. Discriminative approaches try to scale the posteriors based on OOD detection or modify the learning loss function. Intuitively, the easiest solution for OOD confidence calibration is to learn a function that gives higher scores for in-distribution samples and lower scores for OOD samples, and thereby re-scale the posterior or confidence score from the original model accordingly [6]. There are a number of approaches in the literature which try to either modify the loss function [7–9] or adversarially train the network to be less confident on OOD samples [4, 10]. However, one can adversarially manipulate an OOD sample where the model is less confident to find another OOD sample where the model is overconfident [4, 11, 12]. Recently, as shown by Hein et al. [4], the  $\text{ReLU}$  networks produce arbitrarily high confidence as the inference point moves far away from the training data. Therefore, calibrating  $\text{ReLU}$  networks for the whole OOD region is not possible without fundamentally changing the network architecture. As a result, all of the aforementioned algorithms are unable to provide any guarantee about the performance of the network through out the whole feature space. On the other end of the spectrum, the generative group tries

<sup>1</sup> Johns Hopkins University (JHU), <sup>2</sup>Scale AI

\* corresponding author: [jdey4@jhu.edu](mailto:jdey4@jhu.edu)

to learn generative models for both the in-distribution as well as the out-of-distribution samples. The general idea for the generative group is to get likelihoods for a particular sample out of the generative models for both ID and OOD to do likelihood ratio test [13] or control the likelihood for training distribution far away from the training data to detect OOD samples by thresholding. However, it is not obvious how to control likelihoods far away from the training data for powerful generative models like variational autoencoders (VAEs) [14] and generative adversarial networks (GAN) [15]. Moreover, Nalisnick et al. [16] and Hendrycks et al. [10] showed VAEs and GANs can also yield overconfident likelihoods far away from the training data.

The algorithms described so far are concerned with OOD confidence calibration for deep-nets only. However, in this paper, we show that other approaches which partition the feature space, for example random forest, can also suffer from poor confidence calibration both in the ID and the OOD regions. Moreover, the algorithms described above are concerned about the confidence of the algorithms in the OOD region only and they do not address the confidence calibration within the training distribution at all. This issue is addressed separately in a different group of literature [17–19]. In this paper, we consider both calibration problem jointly and propose an approach that achieves good calibration throughout the whole feature space.

In this paper, we conceptualize both random forest and  $\text{ReLU}$  networks as generalized partitioning rules with an affine activation over each polytope. We consider replacing the affine functions learned over the polytopes with Gaussian kernels. We propose two novel kernel density estimation techniques named *Kernel Generative Forest* (KGF) and *Kernel Generative Network* (KGN). We theoretically show that they asymptotically converge to the true training distribution under certain conditions. At the same time, the estimated likelihood from the kernel generative models decreases for samples far away from the training samples. By adding a suitable bias to the kernel density estimate, we can achieve calibrated posterior over the classes in the OOD region. It completely excludes the need for providing OOD training examples to the model. We conduct several simulation and real data studies that show both KGF and KGN are robust against OOD samples while they maintain good performance in the in-distribution region.

**2 Related Works and Our Contributions** There are a number of approaches in the literature which attempt to learn a generative model and control the likelihoods far away from the training data. For example, Ren et al. [13] employed likelihood ratio test for detecting OOD samples. Wan et al. [8] modify the training loss so that the downstream projected features follow a Gaussian distribution. However, there is no guarantee of performance for OOD detection for the above methods. To the best of our knowledge, only Meinke et al. [5] has proposed an approach to guarantee asymptotic performance for OOD detection. They model the training and the OOD distribution using Gaussian mixture models which enable them to control the class conditional posteriors far away. Compared to the aforementioned methods, our approach differs in several ways:

- We address the confidence calibration problems for both  $\text{ReLU}$ -nets and random forests from a common ground.
- We address in-distribution (ID) and out-of-distribution (OOD) calibration problem as a continuum rather than two separate problems.
- We provide guarantees for asymptotic convergence of our proposed approach under certain conditions for both ID and OOD regions.
- We propose an unsupervised OOD calibration approach, i.e., we do not need to train exhaustively on different OOD samples.

### 3 Methods

**3.1 Setting** Consider a supervised learning problem with independent and identically distributed training samples  $\{(\mathbf{x}_i, y_i)\}_{i=1}^n$  such that  $(X, Y) \sim P_{X,Y}$ , where  $X \sim P_X$  is a  $\mathcal{X} \subseteq \mathbb{R}^d$  valued input and  $Y \sim P_Y$  is a  $\mathcal{Y} = \{1, \dots, K\}$  valued class label. We define in-distribution region as the high density region of  $P_{X,Y}$  and denote it by  $\mathcal{S}$ . Here the goal is to learn a confidence score,  $\mathbf{g} : \mathbb{R}^d \rightarrow [0, 1]^K$ ,  $\mathbf{g}(\mathbf{x}) = [g_1(\mathbf{x}), g_2(\mathbf{x}), \dots, g_K(\mathbf{x})]$  such that,

$$(1) \quad g_y(\mathbf{x}) = \begin{cases} P_{Y|X}(y|\mathbf{x}), & \text{if } \mathbf{x} \in \mathcal{S} \\ P_Y(y), & \text{if } \mathbf{x} \notin \mathcal{S} \end{cases}, \quad \forall y \in \mathcal{Y}$$

where  $P_{Y|X}(y|\mathbf{x})$  is the posterior probability for class  $y$  given by the Bayes formula:

$$(2) \quad P_{Y|X}(y|\mathbf{x}) = \frac{P_{X|Y}(\mathbf{x}|y)P_Y(y)}{\sum_{k=1}^K P_{X|Y}(\mathbf{x}|k)P_Y(k)}, \quad \forall y \in \mathcal{Y}.$$

Here  $P_{X|Y}(\mathbf{x}|y)$  is the class conditional density for the training data which we will refer as  $f_y(\mathbf{x})$  hereafter for brevity.

**3.2 Background and Main Idea** Deep discriminative networks partition the feature space  $\mathbb{R}^d$  into a union of  $p$  affine polytopes  $Q_r$  such that  $\bigcup_{r=1}^p Q_r = \mathbb{R}^d$ , and learn an affine function over each polytope [4, 20]. Mathematically, the class-conditional density for the label  $y$  estimated by these deep discriminative models at a particular point  $\mathbf{x}$  can be expressed as:

$$(3) \quad \hat{f}_y(\mathbf{x}) = \sum_{r=1}^p (\mathbf{a}_r^\top \mathbf{x} + b_r) \mathbb{1}(\mathbf{x} \in Q_r).$$

For example, in the case of a decision tree,  $\mathbf{a}_r = \mathbf{0}$ , i.e., decision tree assumes uniform distribution for the class-conditional densities over the leaf nodes. Among these polytopes, the ones that lie on the boundary of the training data extend to the whole feature space and hence encompass all the OOD samples. Since the posterior probability for a class is determined by the affine activation over each of these polytopes, the algorithms tend to be overconfident when making predictions on the OOD inputs. Moreover, there exist some polytopes that are not populated with training data. These unpopulated polytopes serve to interpolate between the training sample points. If we replace the affine activation function of the populated polytopes with Gaussian kernel  $\mathcal{G}$  learned using maximum likelihood approach on the training points within the corresponding polytope and prune the unpopulated ones, the tail of the kernel will help interpolate between the training sample points while assigning lower likelihood to the low density or unpopulated polytope regions of the feature space. This may result in better confidence calibration for the proposed modified approach.

**3.3 Proposed Model** Consider the collection of polytope indices  $\mathcal{P}$  which contains the indices of total  $\tilde{p}$  polytopes populated by the training data. We consider replacing the affine function over the populated polytopes with a Gaussian kernel  $\mathcal{G}(\cdot; \hat{\mu}_r, \hat{\Sigma}_r)$ . For a particular inference point  $\mathbf{x}$ , we consider the Gaussian kernel with the minimum distance from the center of the kernel to the corresponding point:

$$(4) \quad r_{\mathbf{x}}^* = \underset{r}{\operatorname{argmin}} \|\mu_r - \mathbf{x}\|,$$

where  $\|\cdot\|$  denotes a suitable distance measure. We use Euclidean distance metric while conducting the simulation and the benchmark datasets experiments in this paper for simplicity. In short, we modify Equation 3 from the parent R<sub>ELU</sub>-net or random forest to estimate the class-conditional density as:

$$(5) \quad \tilde{f}_y(\mathbf{x}) = \frac{1}{n_y} \sum_{r \in \mathcal{P}} n_{ry} \mathcal{G}(\mathbf{x}; \mu_r, \Sigma_r) \mathbb{1}(r = r_{\mathbf{x}}^*),$$

where  $n_y$  is the total number of samples with label  $y$  and  $n_{ry}$  is the number of samples from class  $y$  that end up in polytope  $Q_r$ . We add a bias to the class conditional density  $\tilde{f}_y$ :

$$(6) \quad \hat{f}_y(\mathbf{x}) = \tilde{f}_y(\mathbf{x}) + \frac{b}{\log(n)}.$$

Note that in Equation 6,  $\frac{b}{\log(n)} \rightarrow 0$  as the total training points,  $n \rightarrow \infty$ . The class posterior probability (confidence)  $\hat{g}_y(\mathbf{x})$  of class  $y$  for a test point  $\mathbf{x}$  is estimated using the Bayes rule as follows:

$$(7) \quad \hat{g}_y(\mathbf{x}) = \frac{\hat{f}_y(\mathbf{x}) \hat{P}_Y(y)}{\sum_{k=1}^K \hat{f}_k(\mathbf{x}) \hat{P}_Y(k)},$$

where  $\hat{P}_Y(y)$  is the empirical prior probability of class  $y$  estimated from the training data. We estimate the class for a particular inference point  $\mathbf{x}$  as:

$$(8) \quad \hat{y} = \operatorname{argmax}_{y \in \mathcal{Y}} \hat{g}_y(\mathbf{x}).$$

**3.4 Desiderata** We desire our proposed model to estimate confidence score  $\hat{g}_y$  to satisfy the following two desiderata:

1. **Asymptotic Performance:** We want point-wise convergence for our estimated confidence as  $n \rightarrow \infty$ , i.e.,

$$\max_{y \in \mathcal{Y}} \sup_{\mathbf{x} \in \mathbb{R}^d} |g_y(\mathbf{x}) - \hat{g}_y(\mathbf{x})| \rightarrow 0.$$

2. **Finite Sample Performance:** We want better posterior calibration for  $\hat{g}_y(\mathbf{x})$  both in ID and OOD region compared to that of its parent model.

We theoretically derive the conditions under which we achieve Desiderata 1 in Section 4. However, we run extensive experiments on various simulation and benchmark datasets in Section 6 to empirically verify that our proposed approach achieves Desiderata 2.

## 4 Theoretical Results

**Theorem 1 (Asymptotic Convergence to the True Distribution).** *Consider a partition rule that partitions  $\mathbb{R}^d$  into hypercubes of the same size  $h_n > 0$ . Formally, let  $\mathcal{P}_n = \{Q_1, Q_2, \dots\}$  be a partition of  $\mathbb{R}^d$ , that is, it partitions  $\mathbb{R}^d$  into sets of the type  $\Pi_{i=1}^d [\psi_i h_n, (\psi_i + 1) h_n)$ , where  $\psi_i$ 's are integers. Let  $n$  be the total number of samples and  $n_r$  be the number of data points within polytope  $Q_r$ . Consider the probability density  $f$  estimated for the samples populating the polytopes using Equation 5, denoted as  $\hat{f}$ . The conditions for choosing the Gaussian kernel parameters are:*

1. *The center of the kernel can be any point  $z_r$  within the polytope  $Q_r$  as  $n \rightarrow \infty$ ,*
2. *The kernel bandwidth along any dimension  $\sigma_r$  is any positive number always bounded by the polytope bandwidth  $h_n$  as  $n \rightarrow \infty$ , i.e.,  $\sigma_r = C_r h_n$ , where  $0 < C_r \leq 1$ .*

Consider the following assumptions as well:

1. The polytope bandwidth  $h_n \rightarrow 0$  as  $n \rightarrow \infty$ .
2.  $n$  grows faster than the shrinkage of  $h_n$ , i.e.,  $nh_n \rightarrow \infty$  as  $h_n \rightarrow 0$  in probability.

Given these assumptions, we have that as  $n \rightarrow \infty$ :

$$\sup_{\mathbf{x} \in \mathbb{R}^d} |f(\mathbf{x}) - \hat{f}(\mathbf{x})| \rightarrow 0,$$

where  $|\cdot|$  denotes absolute value of the scalar it operates on.

*Proof.* Please see Appendix A for the proof. ■

**Theorem 2 (Asymptotic OOD Convergence).** Given  $n$  independent and identically distributed training samples  $\{(\mathbf{x}_i, y_i)\}_{i=1}^n$ , we define the distance of an inference point  $\mathbf{x}$  from the training points as:

$$(9) \quad d_{\mathbf{x}} = \min_{i=1, \dots, n} \|\mathbf{x} - \mathbf{x}_i\|.$$

Here  $\|\cdot\|$  denotes a suitable distance measure as mentioned in Equation 4. Given non-zero and bounded bandwidth of the Gaussians, then we have almost sure convergence for  $\hat{g}_y$  as:  $\hat{g}_y(\mathbf{x}) \xrightarrow{as} \hat{P}_Y(y)$  as  $d_{\mathbf{x}} \rightarrow \infty$ .

*Proof.* Please see Appendix A for the proof. ■

**Corollary 3.** Given the conditions in Theorem 1 and 2, we have:

$$\max_{y \in \mathcal{Y}} \sup_{\mathbf{x} \in \mathbb{R}^d} |g_y(\mathbf{x}) - \hat{g}_y(\mathbf{x})| \rightarrow 0.$$

*Proof.* Using the law of large numbers, we have  $\hat{P}_Y(y) = \frac{n_y}{n} \xrightarrow{as} P_Y(y)$  as  $n_y \rightarrow \infty$ . The rest of the proof follows from Theorem 1 and 2. ■

## 5 Model Parameter Estimation

**5.1 Gaussian Kernel Parameter Estimation** Theorem 1 implies that the Gaussian kernel parameters need to maintain two key properties. We use the training data within the polytopes to estimate the Gaussian parameters in a way that we asymptotically satisfy the above two conditions for consistency. To satisfy the first condition, we set the kernel center as:

$$(10) \quad \hat{\mu}_r = \frac{1}{n_r} \sum_{i=1}^n \mathbf{x}_i \mathbb{1}(\mathbf{x}_i \in Q_r).$$

Note that  $\hat{\mu}_r$  in Equation 10 resides always within the corresponding polytope  $Q_r$ . For improving the estimates for the kernel bandwidth, we incorporate the samples from other polytopes  $Q_s$  based on the similarity  $w_{rs}$  between  $Q_r$  and  $Q_s$ . Moreover, We constrain our estimated Gaussian kernels to have diagonal covariance matrix. We use weighted likelihood estimation to estimate the variance  $\Sigma_r$  for a particular polytope  $Q_r$ . For simplicity, we will describe the estimation procedure for  $w_{rs}$  later. The weighted likelihood estimation for  $\Sigma_r$  can be written as:

$$(11) \quad \hat{\Sigma}_r = \underset{\Sigma}{\operatorname{argmin}} - \sum_{i=1}^n \sum_{s \in \mathcal{P}} w_{rs} \mathbb{1}(\mathbf{x}_i \in Q_s) \log \mathcal{G}(\mathbf{x}_i; \hat{\mu}_r, \Sigma) + \lambda \|\Sigma^{-1}\|_F^2,$$

where we regularize the Frobenius norm of precision matrix  $\Sigma^{-1}$  so that  $\Sigma$  does not become singular and  $\lambda$  is the regularization parameter. By solving Equation 11, we find:

$$(12) \quad \hat{\Sigma}_r = \frac{\sum_{s \in \mathcal{P}} \sum_{i=1}^n w_{rs} \mathbb{1}(\mathbf{x}_i \in Q_s) (\mathbf{x}_i - \hat{\mu}_r)(\mathbf{x}_i - \hat{\mu}_r)^\top + \lambda I_d}{\sum_{s \in \mathcal{P}} \sum_{i=1}^n w_{rs} \mathbb{1}(\mathbf{x}_i \in Q_s)},$$

where,  $I_d$  is a  $d$  dimensional identity matrix. However, we want  $\Sigma_r$  to be estimated based on the samples within  $Q_r$  so that the second condition for the Gaussian parameters is satisfied. Therefore, as  $n \rightarrow \infty$  and  $h_n \rightarrow 0$ , the estimated weights  $w_{rs}$  should satisfy the condition:

$$(13) \quad w_{rs} \rightarrow \begin{cases} 0, & \text{if } Q_r \neq Q_s \\ 1, & \text{if } Q_r = Q_s. \end{cases}$$

We need Condition 13 as we will be only using the data within the polytope  $Q_r$  as  $n \rightarrow \infty$  to estimate the Gaussian bandwidth and the estimated Gaussian bandwidth will be bounded by the polytope bandwidth. Additionally, we use weighted samples to replace the ratio  $\frac{n_{ry}}{n_y}$  in Equation 5 as:

$$(14) \quad \frac{\tilde{w}_{ry}}{\tilde{w}_y} = \frac{\tilde{w}_{ry}}{\sum_{r \in \mathcal{P}} \tilde{w}_{ry}} = \frac{\sum_{s \in \mathcal{P}} \sum_{i=1}^n w_{rs} \mathbb{1}(\mathbf{x}_i \in Q_s) \mathbb{1}(y_i = y)}{\sum_{r \in \mathcal{P}} \sum_{s \in \mathcal{P}} \sum_{i=1}^n w_{rs} \mathbb{1}(\mathbf{x}_i \in Q_s) \mathbb{1}(y_i = y)}.$$

Note that if we satisfy Condition 13, then we have  $\frac{\tilde{w}_{ry}}{\tilde{w}_y} \rightarrow \frac{n_{ry}}{n_y}$  as  $n \rightarrow \infty$ . Therefore, we modify Equation 5 as:

$$(15) \quad \tilde{f}_y(\mathbf{x}) = \frac{1}{\tilde{w}_y} \sum_{r \in \mathcal{P}} \tilde{w}_{ry} \mathcal{G}(\mathbf{x}; \hat{\mu}_r, \hat{\Sigma}_r) \mathbb{1}(r = \hat{r}_{\mathbf{x}}^*),$$

where  $\hat{r}_{\mathbf{x}}^* = \operatorname{argmin}_r \|\hat{\mu}_r - \mathbf{x}\|$ . Below, we describe how we estimate  $w_{rs}$  for KGF and KGN.

**5.2 Kernel Generative Forest** Consider  $T$  number of decision trees in a random forest trained on  $n$  i.i.d training samples  $\{(\mathbf{x}_i, y_i)\}_{i=1}^n$ . Each tree  $t$  partitions the feature space into  $p_t$  polytopes resulting in a set of polytopes:  $\{\{Q_{t,r}\}_{r=1}^{p_t}\}_{t=1}^T$ . The intersection of these polytopes gives a new set of polytopes  $\{Q_r\}_{r=1}^p$  for the forest. For any point  $\mathbf{x}_r \in Q_r$ , we push every other sample point  $\mathbf{x}_s \in Q_s$  down the trees. Now, we define the weight  $w'_{rs}$  as:

$$(16) \quad w'_{rs} = \frac{t_{rs}}{T},$$

where  $t_{rs}$  is the total number trees  $\mathbf{x}_r$  and  $\mathbf{x}_s$  end up in the same leaf node. Note that  $0 \leq w'_{rs} \leq 1$ . If the two samples end up in the same leaves in all the trees, they belong to the same polytope, i.e.  $Q_r = Q_s$ .

In short,  $w'_{rs}$  is the fraction of total trees where the two samples follow the same path from the root to a leaf node. We exponentiate  $w'_{rs}$  with a suitable function of  $n$  which grows with  $n$  so that Condition 13 is satisfied:

$$(17) \quad w_{rs} = (w'_{rs})^{O(n)}.$$

**5.3 Kernel Generative Network** Consider a fully connected ReLU-net trained on  $n$  i.i.d training samples  $\{(\mathbf{x}_i, y_i)\}_{i=1}^n$ . We have the set of all nodes denoted by  $\mathcal{N}_l$  at a particular layer  $l$ . We can randomly pick a node  $n_l \in \mathcal{N}_l$  from  $\mathcal{A}_l$  at each layer  $l$ , and construct a sequence of nodes starting at the input layer and ending at the output layer which we call an **activation path**:  $m = \{n_l \in \mathcal{N}_l\}_{l=1}^L$ . Note that there are  $N = \prod_{l=1}^L |\mathcal{N}_l|$  possible activation paths for a sample in the ReLU-net, where  $|\cdot|$  denotes the cardinality or the number of elements in the set. We index each path by a unique identifier number  $z \in \mathbb{N}$  and construct a sequence of activation paths as:  $\mathcal{M} = \{m_z\}_{z=1, \dots, N}$ . Therefore,  $\mathcal{M}$  contains all possible activation pathways from the input to the output of the network.

While pushing a training sample  $\mathbf{x}_i$  through the network, we define the activation from a ReLU unit at any node as ‘1’ when it has non-negative input and ‘0’ otherwise. Therefore, the activation indicates on which side of the affine function at each node the sample falls. The activation for all nodes in an activation path  $m_z$  for a particular sample creates an **activation mode**  $a_z \in \{0, 1\}^L$ . If we evaluate the activation mode for all activation paths in  $\mathcal{M}$  while pushing a sample through the network, we get a sequence of activation modes:  $\mathcal{A}_r = \{a_z^r\}_{z=1}^N$ . Here  $r$  is the index of the polytope where the sample falls in.

*If the two sequences of activation modes for two different training samples are identical, they belong to the same polytope.* In other words, if  $\mathcal{A}_r = \mathcal{A}_s$ , then  $Q_r = Q_s$ . This statement holds because the above samples will lie on the same side of the affine function at each node in different layers of the network. Now, we define the weight  $w'_{rs}$  as:

$$(18) \quad w'_{rs} = \frac{\sum_{z=1}^N \mathbb{1}(a_z^r = a_z^s)}{N}.$$

Note that  $0 \leq w'_{rs} \leq 1$ . In short,  $w'_{rs}$  is the fraction of total activation paths which are identically activated for two samples in two different polytopes  $r$  and  $s$ . We exponentiate the weights using Equation 17.

Pseudocodes outlining the two algorithms are provided in Appendix C.

**6 Experimental Results** We conduct several experiments on two dimensional simulated datasets and OpenML-CC18 data suite [21]<sup>1</sup> to gain insights on the finite sample performance of KGF and KGN. The details of the simulation datasets and hyperparameters used for all the experiments are provided in Appendix B. For the simulation setups, we use classification error, hellinger distance [22, 23] from the true class conditional posteriors and mean max confidence or posterior [4] as performance statistics. While measuring in-distribution calibration for the datasets in OpenML-CC18 data suite, as we do not know the true distribution, we used adaptive calibration error as defined by Nixon et al. [24] with a fixed bin number of  $R = 15$  across all the datasets. Given  $n$  OOD samples, we define OOD calibration error to measure OOD performance for the benchmark datasets as:

$$\left| \frac{1}{n} \sum_{i=1}^n \max_{y \in \mathcal{Y}} (\hat{P}_{Y|X}(y|\mathbf{x}_i)) - \max_{y \in \mathcal{Y}} (\hat{P}_Y(y)) \right|.$$

**6.1 Simulation Study** Figure 1 top row shows 10000 training samples with 5000 samples per class sampled within the region  $[-1, 1] \times [-1, 1]$  from the five simulation setups described in Appendix B. Therefore, the empty annular region between  $[-1, 1] \times [-1, 1]$  and  $[-2, 2] \times [-2, 2]$  is the low density or OOD region in Figure 1. The corresponding true posteriors  $\mathbb{P}[Y = 0|X = \mathbf{x}]$  are shown in the

<sup>1</sup><https://www.openml.org/s/99>



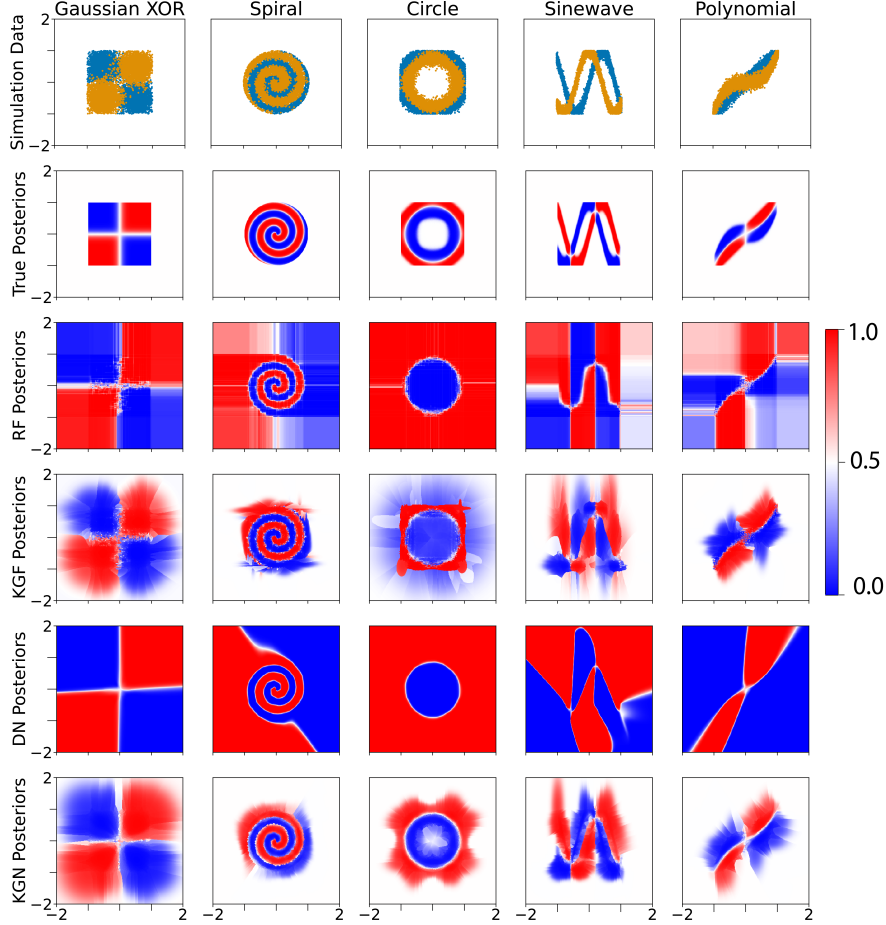


Figure 1: **Visualization of true and estimated posteriors for class 0 from five binary class simulation experiments.** Row 1: 10,000 training points with 5,000 samples per class sampled from 5 different simulation setups for binary class classification. The class labels are indicated by yellow and blue colors. Row 2: True class conditional posteriors. Row 3: Estimated posteriors from random forest. Row 4: Estimated posteriors from KGF. Row 5: Estimated posteriors from Deep-net. Row 6: Estimated posteriors from KGN. The posteriors estimated from KGN and KGF are better calibrated for both in- and out-of-distribution regions compared to those of their parent algorithms.

second row of Figure 1. As shown in Row 3 and 5, RF and DN are really good at estimating the high density regions of training distribution. However, they overestimate the posteriors in the low density regions of training distribution. Row 4 and 6 of Figure 1 show KGF and KGN improves the posterior estimation specially in the low density of the training distribution or OOD regions of the feature space. Because of axis aligned split in random forest RF and thereby, KGF are less efficient in learning non-linear decision boundaries like spiral, circle and sinewave simulations than R&L-net and KGN. Figure 2 quantifies the performance of the algorithms which are visually represented in Figure 1. KGF and KGN maintain similar classification accuracy to those of their parent algorithms. We measure hellinger distance from the true distribution for increasing training sample size within  $[-1, 1] \times [-1, 1]$  region as an index for in-distribution calibration. Column 2 of left and right block in Figure 2 show KGF and KGN are better at estimating the high density region of training distribution compared to their parent methods. For measuring OOD performance, we normalize the training data by the maximum of their  $l_2$  norm so that the training data is confined within a unit circle. For inference, we sample 1000 inference



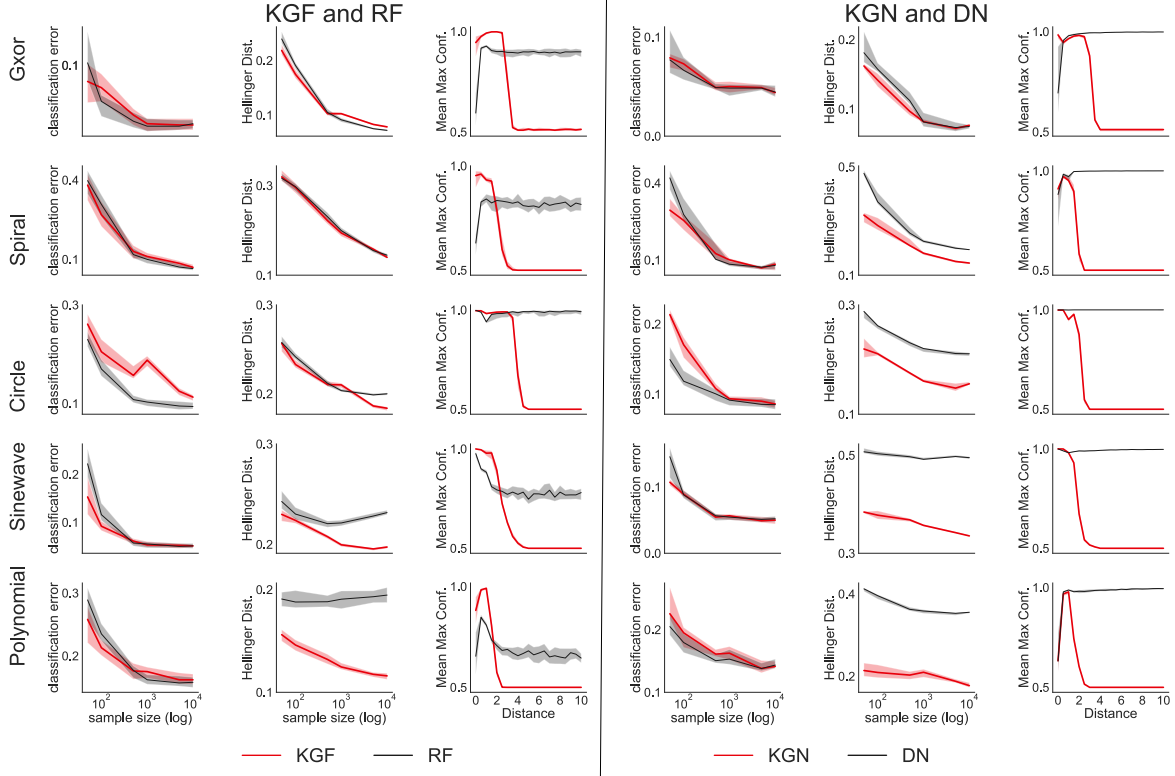


Figure 2: **Classification error, Hellinger distance from true posteriors, mean max confidence or posterior for the simulation experiments.** The median performance is shown as a dark curve with shaded region as error bars showing the 25-th and the 75-th percentile. KGF (Left block) and KGN (Right block) improve both in- and out-of-distribution calibration of their respective parent algorithms while maintaining nearly similar classification accuracy on the simulation datasets.

points uniformly from a circle where the circles have increasing radius and plot mean max posterior for increasing distance from the origin. Therefore, for distance up to 1 we have in-distribution samples and distances farther than 1 can be considered as OOD region. As shown in Column 3 of Figure 2, mean max posteriors or confidence for KGF and KGN converge to the maximum of the class priors, i.e., 0.5 as we go farther away from the training data origin.

**6.2 Benchmark Data Study** We used OpenML-CC18 data suite for benchmark dataset study. We exclude any dataset which contain categorical features or NaN values and conduct our experiments on 46 datasets with varying dimensions and sample sizes. For the OOD experiments, we follow a similar setup as that of the simulation data. We normalize the training data by their maximum  $l_2$  norm and sample 1000 testing samples uniformly from each hypersphere where the hyperspheres have increasing radius starting from 1 to 5. Figure 3 shows the summary of performance of the algorithms. The extended results for each dataset is shown separately in appendix Figure 4, 5, 6, 7, 8 and 9. Figure 3 left column shows on average KGF and KGN has nearly similar classification accuracy to their respective parent algorithm. However, according to Figure 3 middle column, KGF improves the in-distribution calibration for random forest by a huge margin. On the contrary, KGN maintains similar in-distribution calibration performance to that of its parent RReLU-net. Most interestingly, Figure 3 right column KGN and KGF improves OOD calibration of their respective parent algorithms by a huge margin.

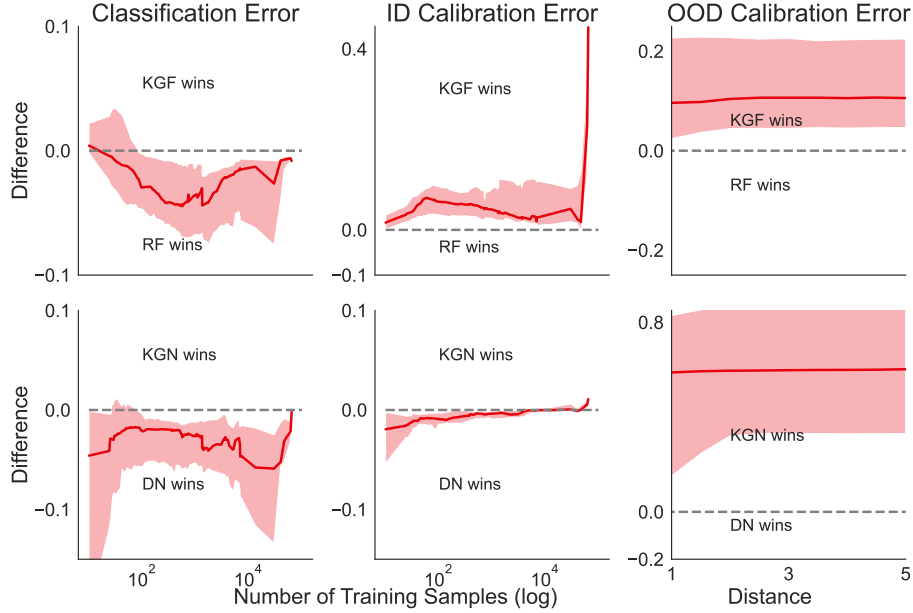


Figure 3: **Performance summary of KGF and KGN on OpenML-CC18 data suite.** The dark red curve in the middle shows the median of performance on 46 datasets. The shaded region shows the error bar consisting of the 25-th and the 75-th percentile of the performance statistics. **Left:** KGF and KGN maintains performance close to their parent algorithms for classification. **Middle:** KGF significantly improves the in-distribution calibration for random forest and KGN improves RReLU-net’s in-distribution calibration for high training sample sizes. **Right:** Both of the proposed approaches yield highly calibrated confidence in the OOD region.

**7 Discussion** In this paper, we convert deep discriminative models to deep generative models by replacing the affine function over the polytopes in the discriminative models with a Gaussian kernel. This replacement of affine function results in better in- and out-of-distribution calibration for our proposed approaches while maintaining classification accuracy close to the parent algorithm. Theoretically, we show under certain conditions our approaches asymptotically converge to the true training distribution and this establishes confidence calibration for learning algorithms in in- and out-of-distribution regions as a continuum rather than two different problems.

For a feature space densely partitioned with small polytopes, we can use Euclidean distance metric in Equation 4. This is because the Euclidean manifold approximation holds locally for the corresponding polytope with index  $r_x^*$ . On the contrary, for a feature space partitioned with large polytopes, Euclidean distance measure may be a wrong notion of distance, specially when the underlying manifold is non-Euclidean. Note that the indicator function in Equation 5 and pruning of the unpopulated polytopes result in an enlargement of the polytopes in our proposed method compared to that of the parent model in Equation 3. Therefore, our proposed approach while using Euclidean metric in Equation 4 may have less classification accuracy compared to that of its parent algorithm. A correct measure of distance in all the cases including the aforementioned non-Euclidean one would be the geodesic distance as explored by Madhyastha et al. [25]. We will explore convolutional neural nets (CNN) trained on image and language benchmark datasets using geodesic distance in Equation 4 in our future work. Additionally, the proposed approach needs benchmarking against other calibration approaches in the literature which are mainly based on image datasets and we will pursue the benchmarking task in our future work.

**Acknowledgements** The authors thank the support of the NSF-Simons Research Collaborations on the Mathematical and Scientific Foundations of Deep Learning (NSSF grant 2031985) and THEORINET. This work is graciously supported by the Defense Advanced Research Projects Agency (DARPA) Lifelong Learning Machines program through contracts FA8650-18-2-7834 and HR0011-18-2-0025. Research was partially supported by funding from Microsoft Research and the Kavli Neuroscience Discovery Institute.

## References

- [1] Chuan Guo, Geoff Pleiss, Yu Sun, and Kilian Q. Weinberger. On calibration of modern neural networks. In Doina Precup and Yee Whye Teh, editors, Proceedings of the 34th International Conference on Machine Learning, volume 70 of Proceedings of Machine Learning Research, pages 1321–1330. PMLR, 06–11 Aug 2017.
- [2] Agustinus Kristiadi, Matthias Hein, and Philipp Hennig. Being bayesian, even just a bit, fixes overconfidence in ReLU networks. In Hal Daumé III and Aarti Singh, editors, Proceedings of the 37th International Conference on Machine Learning, volume 119 of Proceedings of Machine Learning Research, pages 5436–5446. PMLR, 13–18 Jul 2020.
- [3] Haoyin Xu, Kaleab A. Kinfu, Will LeVine, Sambit Panda, Jayanta Dey, Michael Ainsworth, Yu-Chung Peng, Madi Kusmanov, Florian Engert, Christopher M. White, Joshua T. Vogelstein, and Carey E. Priebe. When are Deep Networks really better than Decision Forests at small sample sizes, and how? arXiv preprint arXiv:2108.13637, 2021.
- [4] Matthias Hein, Maksym Andriushchenko, and Julian Bitterwolf. Why relu networks yield high-confidence predictions far away from the training data and how to mitigate the problem. In Proceedings of the IEEE/CVF Conference on Computer Vision and Pattern Recognition, pages 41–50, 2019.
- [5] Alexander Meinke, Julian Bitterwolf, and Matthias Hein. Provably robust detection of out-of-distribution data (almost) for free. arXiv preprint arXiv:2106.04260, 2021.
- [6] Shiyu Liang, Yixuan Li, and Rayadurgam Srikant. Enhancing the reliability of out-of-distribution image detection in neural networks. arXiv preprint arXiv:1706.02690, 2017.
- [7] Jay Nandy, Wynne Hsu, and Mong Li Lee. Towards maximizing the representation gap between in-domain & out-of-distribution examples. Advances in Neural Information Processing Systems, 33:9239–9250, 2020.
- [8] Weitao Wan, Yuanyi Zhong, Tianpeng Li, and Jiansheng Chen. Rethinking feature distribution for loss functions in image classification. In Proceedings of the IEEE conference on computer vision and pattern recognition, pages 9117–9126, 2018.
- [9] Terrance DeVries and Graham W Taylor. Learning confidence for out-of-distribution detection in neural networks. arXiv preprint arXiv:1802.04865, 2018.
- [10] Dan Hendrycks, Mantas Mazeika, and Thomas Dietterich. Deep anomaly detection with outlier exposure. arXiv preprint arXiv:1812.04606, 2018.
- [11] Anh Nguyen, Jason Yosinski, and Jeff Clune. Deep neural networks are easily fooled: High confidence predictions for unrecognizable images. In Proceedings of the IEEE conference on computer vision and pattern recognition, pages 427–436, 2015.
- [12] Vikash Sehwal, Arjun Nitin Bhagoji, Liwei Song, Chawin Sitawarin, Daniel Cullina, Mung Chiang, and Prateek Mittal. Better the devil you know: An analysis of evasion attacks using out-of-distribution adversarial examples. arXiv preprint arXiv:1905.01726, 2019.

- [13] Jie Ren, Peter J Liu, Emily Fertig, Jasper Snoek, Ryan Poplin, Mark Depristo, Joshua Dillon, and Balaji Lakshminarayanan. Likelihood ratios for out-of-distribution detection. Advances in neural information processing systems, 32, 2019.
- [14] Diederik P Kingma, Max Welling, et al. An introduction to variational autoencoders. Foundations and Trends® in Machine Learning, 12(4):307–392, 2019.
- [15] Ian Goodfellow, Jean Pouget-Abadie, Mehdi Mirza, Bing Xu, David Warde-Farley, Sherjil Ozair, Aaron Courville, and Yoshua Bengio. Generative adversarial networks. Communications of the ACM, 63(11):139–144, 2020.
- [16] Eric Nalisnick, Akihiro Matsukawa, Yee Whye Teh, Dilan Gorur, and Balaji Lakshminarayanan. Do deep generative models know what they don't know? arXiv preprint arXiv:1810.09136, 2018.
- [17] Chuan Guo, Geoff Pleiss, Yu Sun, and Kilian Q Weinberger. On calibration of modern neural networks. In International conference on machine learning, pages 1321–1330. PMLR, 2017.
- [18] Richard Guo, Ronak Mehta, Jesus Arroyo, Hayden Helm, Cencheng Shen, and Joshua T Vogelstein. Estimating information-theoretic quantities with uncertainty forests. arXiv, pages arXiv–1907, 2019.
- [19] Meelis Kull, Miquel Perello Nieto, Markus Kängsepp, Telmo Silva Filho, Hao Song, and Peter Flach. Beyond temperature scaling: Obtaining well-calibrated multi-class probabilities with dirichlet calibration. Advances in neural information processing systems, 32, 2019.
- [20] Haoyin Xu, Kaleab A Kinfu, Will LeVine, Sambit Panda, Jayanta Dey, Michael Ainsworth, Yu-Chung Peng, Madi Kusmanov, Florian Engert, Christopher M White, et al. When are deep networks really better than decision forests at small sample sizes, and how? arXiv preprint arXiv:2108.13637, 2021.
- [21] Bernd Bischl, Giuseppe Casalicchio, Matthias Feurer, Pieter Gijsbers, Frank Hutter, Michel Lang, Rafael G Mantovani, Jan N van Rijn, and Joaquin Vanschoren. Openml benchmarking suites. arXiv preprint arXiv:1708.03731, 2017.
- [22] Thomas Kailath. The divergence and bhattacharyya distance measures in signal selection. IEEE transactions on communication technology, 15(1):52–60, 1967.
- [23] C Radhakrishna Rao. A review of canonical coordinates and an alternative to correspondence analysis using hellinger distance. Qüestiió: quaderns d'estadística i investigació operativa, 1995.
- [24] Jeremy Nixon, Michael W Dusenberry, Linchuan Zhang, Ghassen Jerfel, and Dustin Tran. Measuring calibration in deep learning. In CVPR workshops, volume 2, 2019.
- [25] Meghana Madhyastha, Gongkai Li, Veronika Strnadová-Neeley, James Browne, Joshua T Vogelstein, Randal Burns, and Carey E Priebe. Geodesic forests. In Proceedings of the 26th ACM SIGKDD International Conference on Knowledge Discovery & Data Mining, pages 513–523, 2020.

## Appendix A. Proofs.

**A.1 Proof of Theorem 1** Consider the density estimator for the samples populating the polytopes  $\hat{f}$ . Let  $n$  be the total number of samples and  $n_r$  be the number of data points within polytope  $Q_r$ . As stated in the theorem statement, we make the following assumptions:

1. The polytope bandwidth  $h_n \rightarrow 0$  as  $n \rightarrow \infty$ .
2.  $n$  grows faster than the shrinkage of  $h_n$ , i.e.,  $n \cdot h_n \rightarrow \infty$  as  $h_n \rightarrow 0$  in probability.

For simplicity, we first explore the one-dimensional distribution. The derivation can be readily extended to multi-dimensional scenarios. We consider any Gaussian kernel  $\mathcal{G}'()$  with parameters chosen independently of the data satisfying two conditions. In lemma 4 and 5, we will show that the aforementioned class of estimators is consistent. The conditions for choosing the Gaussian kernel parameters are:

1. The center of the kernel can be any point  $z_r$  within the polytope  $Q_r$  as  $n \rightarrow \infty$ ,
2. The kernel bandwidth  $\sigma_r$  is any non-negative number always bounded by the polytope bandwidth  $h_n$  as  $n \rightarrow \infty$ , i.e.,  $\sigma_r = C_r h_n$ , where  $0 < C_r \leq 1$ .

Now the class conditional density estimate at a point  $x$  can be written as:

$$(19) \quad \hat{f}(x) = \frac{1}{n} \sum_{r \in \mathcal{P}} n_r \mathcal{G}'(x; \mu_r, \Sigma_r) \mathbb{1}(r = r_x^*).$$

**Lemma 4.** *The class of estimators in (19) is an asymptotically unbiased class of estimators of the true density  $f$ .*

**Proof.** The polytope sample counts  $n_r$  can be considered as binomially distributed:  $n_r \sim B(n, P_r)$ , where  $P_r = \int_{Q_r} dF$  is the probability of finding a training sample within the polytope  $r$  and  $F$  is the cumulative density function associated with the density  $f$ . This allows us to write:  $\mathbb{E}[n_r] = n P_r$ . Using the mean value theorem, we have that  $P_r = h_n f(q_r)$ , for some  $q_r \in Q_r$ . Note that, if we consider the multi-dimensional scenario for the mean value theorem here, the proof can be easily generalized for multi-dimensional case.

Now consider the expectation of  $\hat{f}$  with respect to the training distribution:

$$(20) \quad \mathbb{E}[\hat{f}(x)] = \sum_{r \in \mathcal{P}} \frac{n P_r \mathcal{G}'(x; \mu_r, \Sigma_r) \mathbb{1}(r = r_x^*)}{n} = \sum_{r \in \mathcal{P}} h_n f(q_r) \mathcal{G}'(x; \mu_r, \Sigma_r) \mathbb{1}(r = r_x^*).$$

Note that we are given the partitions of the feature space and we choose Gaussian parameters such that they are independent of the training data. Therefore,  $\mathcal{G}'(x, \mu_r, \Sigma_r) \mathbb{1}(r = r_x^*)$  is not a random variable. Now, as  $n \rightarrow \infty$ ,  $h_n \rightarrow 0$ , and  $h_n$  can be considered an infinitesimal measure  $dz_r$ . Furthermore, as the bandwidth of the Gaussian is limited by the polytope bandwidth and the area under the Gaussian is 1, the kernel  $\mathcal{G}'(x, \mu_r, \Sigma_r) \mathbb{1}(r = r_x^*)$  becomes a dirac delta function evaluated at  $x$  as  $h_n \rightarrow 0$ . Therefore, in the limiting conditions,  $\mathcal{G}'(x, \mu_r, \Sigma_r) \mathbb{1}(r = r_x^*) \rightarrow \delta(x - z_r)$  and  $f(q_r) \rightarrow f(z_r)$ . Here  $z_r$  is a point such that  $z_r \in Q_r$  for all  $n$ . As  $n \rightarrow \infty$ , the summation in (20) thus becomes an integral over the space  $\mathbb{R}$ . Therefore, in the limit we can write 20 as

$$(21) \quad \begin{aligned} \mathbb{E}[\hat{f}(x)] &= \int_{-\infty}^{\infty} f(z_r) \delta(x - z_r) dz_r \\ &= f(x) \end{aligned}$$

Therefore,  $\hat{f}(x)$  is an asymptotically unbiased estimator of  $f(x)$ . ■

**Lemma 5.** *The variance of the class of estimators in (19) asymptotically goes to 0.*

**Proof.** For binomially distributed samples  $n_r$ , we can write,  $\mathbb{V}ar[n_r] = nP_r(1 - P_r)$ . Therefore, we can estimate the variance of  $\hat{f}(x)$  as:

$$\begin{aligned}
 \mathbb{V}ar[\hat{f}(x)] &= \sum_{r \in \mathcal{P}} \frac{nP_r(1 - P_r)}{n^2} \{\mathcal{G}'(x; \mu_r, \Sigma_r) \mathbb{1}(r = r_x^*)\}^2 \\
 &= \frac{h_n f(z_{r_x^*})(1 - h_n f(z_{r_x^*}))}{n} \left\{ \frac{1}{\sqrt{2\pi}\sigma_{r_x^*}} \exp\left(-\frac{(x - \mu_{r_x^*})^2}{2\sigma_{r_x^*}^2}\right) \right\}^2 \\
 &= \frac{h_n f(z_{r_x^*})(1 - h_n f(z_{r_x^*}))}{nC_{r_x^*}^2 h_n^2} \left\{ \frac{1}{\sqrt{2\pi}} \exp\left(-\frac{(x - \mu_{r_x^*})^2}{2\sigma_{r_x^*}^2}\right) \right\}^2 \\
 &\leq \frac{f(z_{r_x^*})(1 - h_n f(z_{r_x^*}))}{2\pi C_{r_x^*}^2 (nh_n)}
 \end{aligned} \tag{22}$$

Equation 22 offers several interesting insights:

1. As  $h_n \rightarrow 0$ ,  $z_{r_x^*} \rightarrow x$  and  $f(z_{r_x^*})(1 - h_n f(z_{r_x^*})) \rightarrow f(x)$ . Therefore, the variance becomes directly dependent on  $f(x)$ . There is more variability at regions with higher density.

2. The variance is also higher if  $C_{r_x^*}^2 \ll 1$ . Therefore,  $C_{r_x^*}$  should be as close to 1 as possible and  $nh_n$  should be as high as possible for lower variance. Moreover, variance can be reduced at the expense of higher bias with  $C_{r_x^*} > 1$ . Most importantly note that, the effect of  $C_{r_x^*}$  cancels out in the numerator and the denominator while estimating the posteriors in Equation 7.

3. As  $h_n \rightarrow 0$  the estimation becomes unbiased (see Equation 20), but the estimation variance becomes unbounded. Therefore, for bounded and decreasing variance the condition  $nh_n \rightarrow \infty$  is necessary. ■

Lemma 4 and 5 together completes the proof of Theorem 1.

**A.2 Proof of Theorem 2** We first expand  $\hat{g}_y(\mathbf{x})$ :

$$\begin{aligned}
 \hat{g}_y(\mathbf{x}) &= \frac{\hat{f}_y(\mathbf{x}) \hat{P}_Y(y)}{\sum_{k=1}^K \hat{f}_k(x) \hat{P}_Y(k)} \\
 &= \frac{\hat{f}_y(\mathbf{x}) \hat{P}_Y(y) + \frac{b}{\log(n)} \hat{P}_Y(y)}{\sum_{k=1}^K (\hat{f}_k(\mathbf{x}) \hat{P}_Y(k) + \frac{b}{\log(n)} \hat{P}_Y(k))}
 \end{aligned}$$

As the inference point  $\mathbf{x}$  becomes more distant from training samples (and more distant from all of the Gaussian centers), we have that  $\mathcal{G}(\mathbf{x}, \hat{\mu}_r, \hat{\Sigma}_r)$  becomes smaller. Thus,  $\forall y, \tilde{f}_y(\mathbf{x})$  shrinks. More formally,  $\forall y$ ,

$$\lim_{d_{\mathbf{x}} \rightarrow \infty} \tilde{f}_y(\mathbf{x}) = 0$$

We can use this result to then examine the limiting behavior of our posteriors as the inference point  $\mathbf{x}$  becomes more distant from the training data:

$$\begin{aligned}
\lim_{d_{\mathbf{x}} \rightarrow \infty} \hat{g}_y(\mathbf{x}) &= \lim_{d_{\mathbf{x}} \rightarrow \infty} \frac{\tilde{f}_y(\mathbf{x})\hat{P}_Y(y) + \frac{b}{\log(n)}\hat{P}_Y(y)}{\sum_{k=1}^K (\tilde{f}_k(\mathbf{x})\hat{P}_Y(k) + \frac{b}{\log(n)}\hat{P}_Y(k))} \\
&= \frac{(\lim_{d_{\mathbf{x}} \rightarrow \infty} \tilde{f}_y(\mathbf{x}))\hat{P}_Y(y) + \frac{b}{\log(n)}\hat{P}_Y(y)}{\sum_{k=1}^K (\lim_{d_{\mathbf{x}} \rightarrow \infty} \tilde{f}_k(\mathbf{x}))\hat{P}_Y(k) + \frac{b}{\log(n)}\hat{P}_Y(k)} \\
&= \frac{\hat{P}_Y(y)}{\sum_{k=1}^K \hat{P}_Y(k)} \\
&= \hat{P}_Y(y)
\end{aligned}$$

**Appendix B. Simulations.** We construct five types of binary class simulations:

- *Gaussian XOR* is a two-class classification problem with equal class priors. Conditioned on being in class 0, a sample is drawn from a mixture of two Gaussians with means  $\pm[0.5, -0.5]^\top$  and standard deviations of 0.25. Conditioned on being in class 1, a sample is drawn from a mixture of two Gaussians with means  $\pm[0.5, -0.5]^\top$  and standard deviations of 0.25.
- *Spiral* is a two-class classification problem with the following data distributions: let  $K$  be the number of classes and  $S \sim \text{multinomial}(\frac{1}{K}\mathbf{1}_K, n)$ . Conditioned on  $S$ , each feature vector is parameterized by two variables, the radius  $r$  and an angle  $\theta$ . For each sample,  $r$  is sampled uniformly in  $[0, 1]$ . Conditioned on a particular class, the angles are evenly spaced between  $\frac{4\pi(k-1)t_K}{K}$  and  $\frac{4\pi(k)t_K}{K}$ , where  $t_K$  controls the number of turns in the spiral. To inject noise along the spirals, we add Gaussian noise to the evenly spaced angles  $\theta' : \theta = \theta' + \mathcal{N}(0, 0.09)$ . The observed feature vector is then  $(r \cos(\theta), r \sin(\theta))$ .
- *Circle* is a two-class classification problem with equal class priors. Conditioned on being in class 0, a sample is drawn from a circle centered at  $(0, 0)$  with a radius of  $r = 0.75$ . Conditioned on being in class 1, a sample is drawn from a circle centered at  $(0, 0)$  with a radius of  $r = 1$ , which is cut off by the region bounds. To inject noise along the circles, we add Gaussian noise to the circle radii  $r' : r = r' + \mathcal{N}(0, 0.01)$ .
- *Sinewave* is a two-class classification problem based on sine waves. Conditioned on being in class 0, a sample is drawn from the distribution  $y = \cos(\pi x)$ . Conditioned on being in class 1, a sample is drawn from the distribution  $y = \sin(\pi x)$ . We inject Gaussian noise to the sine wave heights  $y' : y = y' + \mathcal{N}(0, 0.01)$ .
- *Polynomial* is a two-class classification problem with the following data distributions:  $y = x^a$ . Conditioned on being in class 0, a sample is drawn from the distribution  $y = x^1$ . Conditioned on being in class 1, a sample is drawn from the distribution  $y = x^3$ . Gaussian noise is added to variables  $y' : y = y' + \mathcal{N}(0, 0.01)$ .

**Appendix C. Pseudocodes.** In this section, we provide the pseudocode for our proposed algorithms.

**Appendix D. Hardware and Software Configurations.**

- Operating System: Linux (ubuntu 20.04), macOS (Ventura 13.2.1)
- VM Size: Azure Standard D96as v4 (96 vcpus, 384 GiB memory)
- GPU: Apple M1 Max
- Software: Python 3.8, scikit-learn  $\geq 0.22.0$ , tensorflow-macos  $\leq 2.9$ , tensorflow-metal  $\leq 0.5.0$ .



Table 1: Hyperparameters for RF and KGF.

Hyperparameters	Value
n_estimators	500
max_depth	$\infty$
min_samples_leaf	1
$O(n)$	$1 + \lfloor \log(n)/3 \rfloor$
$b$ (bias)	$\exp(-10^{\sqrt{d}})$
$\lambda$	$1 \times 10^{-6}$

Table 2: Hyperparameters for ReLU-net and KGN.

Hyperparameters	Value
number of hidden layers	4
nodes per hidden layer	1000
optimizer	Adam
learning rate	$3 \times 10^{-4}$
$O(n)$	$\log_2(n)$
$b$ (bias)	$\exp(-10^{\sqrt{d}})$
$\lambda$	$1 \times 10^{-6}$

---

**Algorithm 1** Fit a KGX model.

---

**Input:**

- (1)  $\theta$  ▷ Parent learner (random forest or deep network model)
- (2)  $\mathcal{D}_n = (\mathbf{X}, \mathbf{y}) \in \mathbb{R}^{n \times d} \times \{1, \dots, K\}^n$  ▷ Training data

**Output:**  $\mathcal{G}$  ▷ a KGX model

```
1: function KGX.FIT( $\theta, \mathbf{X}, \mathbf{y}$ )
2:   for  $i = 1, \dots, n$  do ▷ Iterate over the dataset to calculate the weights
3:     for  $j = 1, \dots, n$  do
4:        $w_{ij} \leftarrow \text{COMPUTEWEIGHTS}(\mathbf{x}_i, \mathbf{x}_j, \theta)$ 
5:     end for
6:   end for
7:
8:
9:    $\{Q_r\}_{r=1}^{\tilde{p}} \leftarrow \text{GETPOLYTOPES}(\mathbf{w})$  ▷ Identify the polytopes by clustering the samples with similar weight
10:
11:    $\mathcal{G}.\{\tilde{w}_k\}_{k=1}^K \leftarrow 0$  ▷ Initialize the counts for each class
12:   for  $r = 1, \dots, \tilde{p}$  do ▷ Iterate over each polytope
13:     for  $k = 1, \dots, K$  do
14:        $\mathcal{G}.\tilde{w}_{rk} \leftarrow \text{COUNTWEIGHTS}(\{\mathbf{w}_{rs}\}_{s=1}^{\tilde{p}}, k)$  ▷  $w_{rk}$  is the number of weighted input samples in  $Q_r$  with label  $k$ 
15:        $\mathcal{G}.\tilde{w}_k \leftarrow \mathcal{G}.\tilde{w}_k + \mathcal{G}.\tilde{w}_{rk}$  ▷ Update the total count for each class
16:     end for
17:      $\mathcal{G}.\hat{\mu}_r, \mathcal{G}.\hat{\Sigma}_r \leftarrow \text{ESTIMATEPARAMETERS}(\mathbf{X}, \{\mathbf{w}_{rs}\}_{s=1}^{\tilde{p}})$  ▷ Fit Gaussians using weighted MLE
18:   end for
19:   return  $\mathcal{G}$ 
20: end function
```

---

---

**Algorithm 2** Computing weights in KGF

---

**Input:**

- (1)  $\mathbf{x}_i, \mathbf{x}_j \in \mathbb{R}^{1 \times d}$  ▷ two input samples to be weighted
- (2)  $\theta$  ▷ parent random forest with  $T$  trees

**Output:**  $w_{ij} \in [0, 1]$  ▷ compute similarity between  $i$  and  $j$ -th samples.

```
1: function COMPUTEWEIGHTS( $\mathbf{x}_i, \mathbf{x}_j, \theta$ )
2:    $\mathcal{I}_i \leftarrow \text{PUSHDOWNTREES}(\mathbf{x}_i, \theta)$  ▷ push  $\mathbf{x}_i$  down  $T$  trees and get the leaf numbers it end up in.
3:    $\mathcal{I}_j \leftarrow \text{PUSHDOWNTREES}(\mathbf{x}_j, \theta)$  ▷ push  $\mathbf{x}_j$  down  $T$  trees and get the leaf numbers it end up in.
4:    $l \leftarrow \text{COUNTMATCHES}(\mathcal{I}_i, \mathcal{I}_j)$  ▷ count the number of times the samples end up in the same leaf
5:    $w_{ij} \leftarrow \frac{l}{T}$ 
6:   return  $w_{ij}$ 
7: end function
```

---

---

**Algorithm 3** Computing weights in KGN
 

---

**Input:**

 (1)  $\mathbf{x}_i, \mathbf{x}_j \in \mathbb{R}^{1 \times d}$ 

▷ two input samples to be weighted

 (2)  $\theta$ 

▷ parent deep-net model

**Output:**  $w_{ij} \in [0, 1]$ 

 ▷ compute similarity between  $i$  and  $j$ -th samples.

 1: **function** COMPUTEWEIGHTS( $\mathbf{x}_i, \mathbf{x}_j, \theta$ )

 2:    $\mathcal{A}_i \leftarrow \text{PUSHDOWNNETWORK}(\mathbf{x}_i, \theta)$ 

 ▷ get activation modes  $\mathcal{A}_i$ 

 3:    $\mathcal{A}_j \leftarrow \text{PUSHDOWNNETWORK}(\mathbf{x}_j, \theta)$ 

 ▷ get activation modes  $\mathcal{A}_j$ 

 4:    $l \leftarrow \text{COUNTMATCHES}(\mathcal{A}_i, \mathcal{A}_j)$ 

▷ count the number of times the two samples activate the

activation paths in a similar way

 5:    $w_{ij} \leftarrow \frac{l}{N}$ 

 ▷  $N$  is the total number of activation paths

 6:   **return**  $w_{ij}$ 

 7: **end function**


---

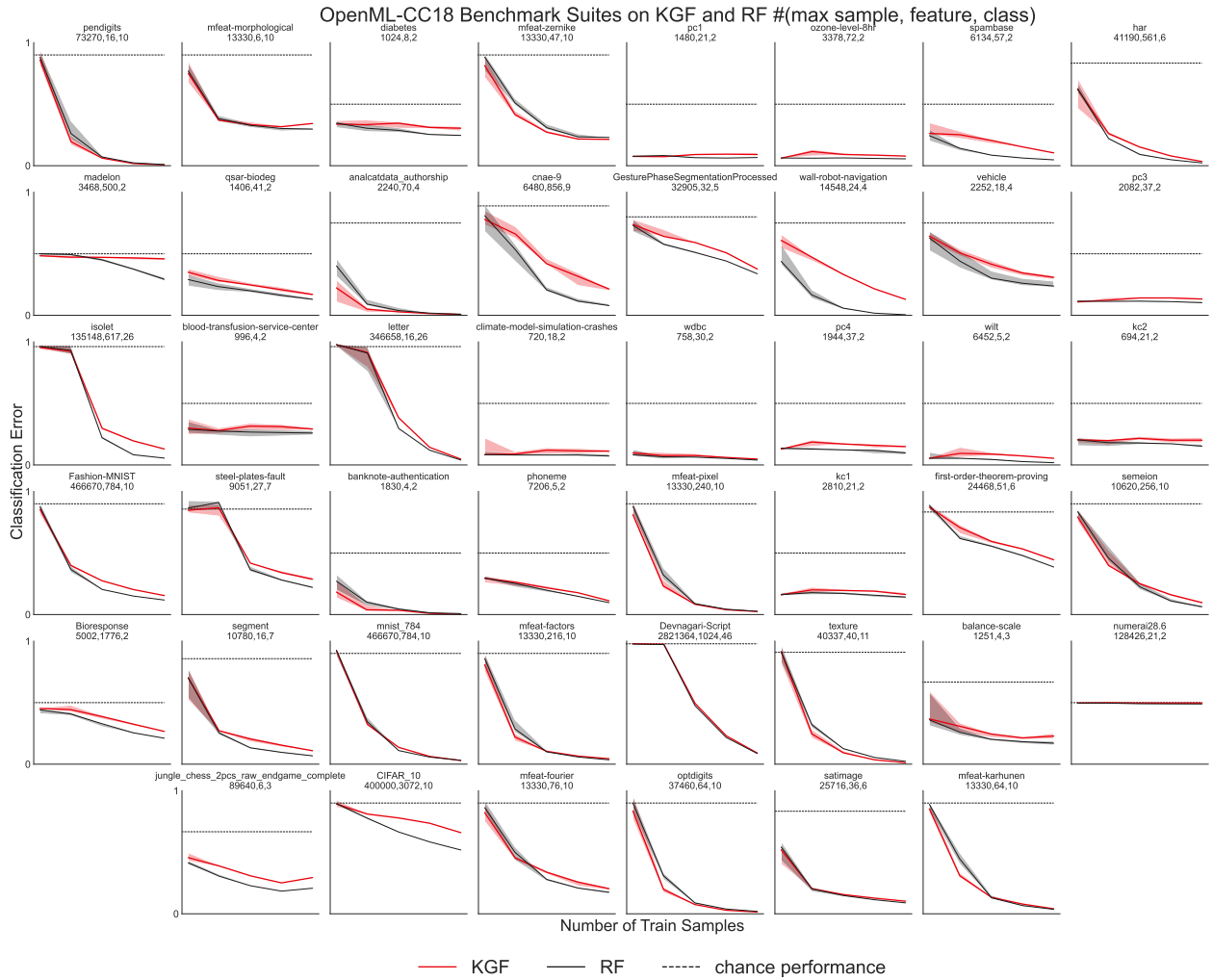


Figure 4: **Extended results on OpenML-CC18 datasets.** Classifications errors for KGF and RF with max sample size, number of features, and number of classes mentioned in the title for each panel.

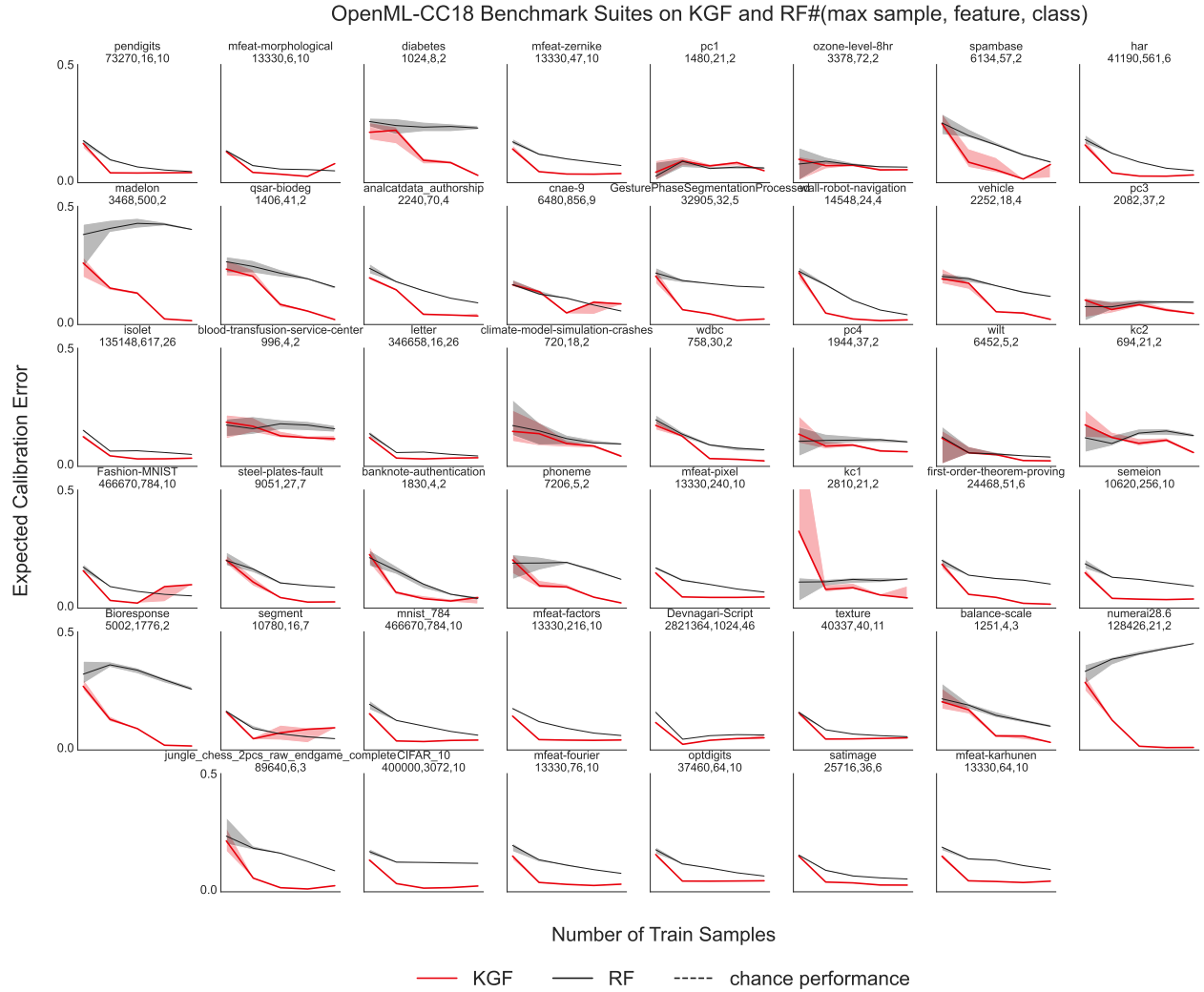


Figure 5: **Extended results on OpenML-CC18 datasets.** Calibration errors for KGF and RF with max sample size, number of features, and number of classes mentioned in the title for each panel.

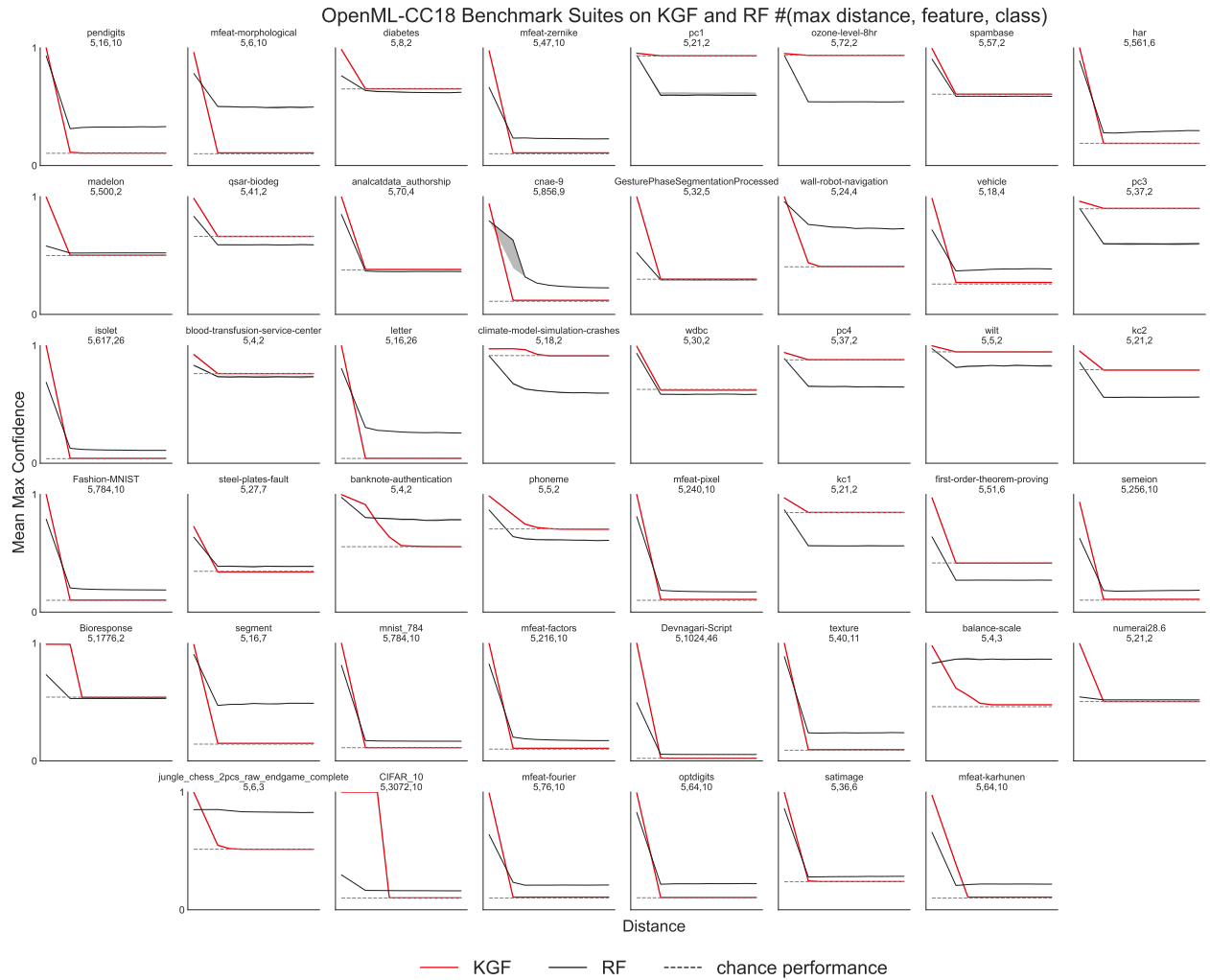


Figure 6: **Extended results on OpenML-CC18 datasets.** Mean max confidence for KGF and RF with max distance from the data origin, number of features, and number of classes mentioned in the title for each panel. The dashed line indicates the maximum of the empirical priors for different class labels.

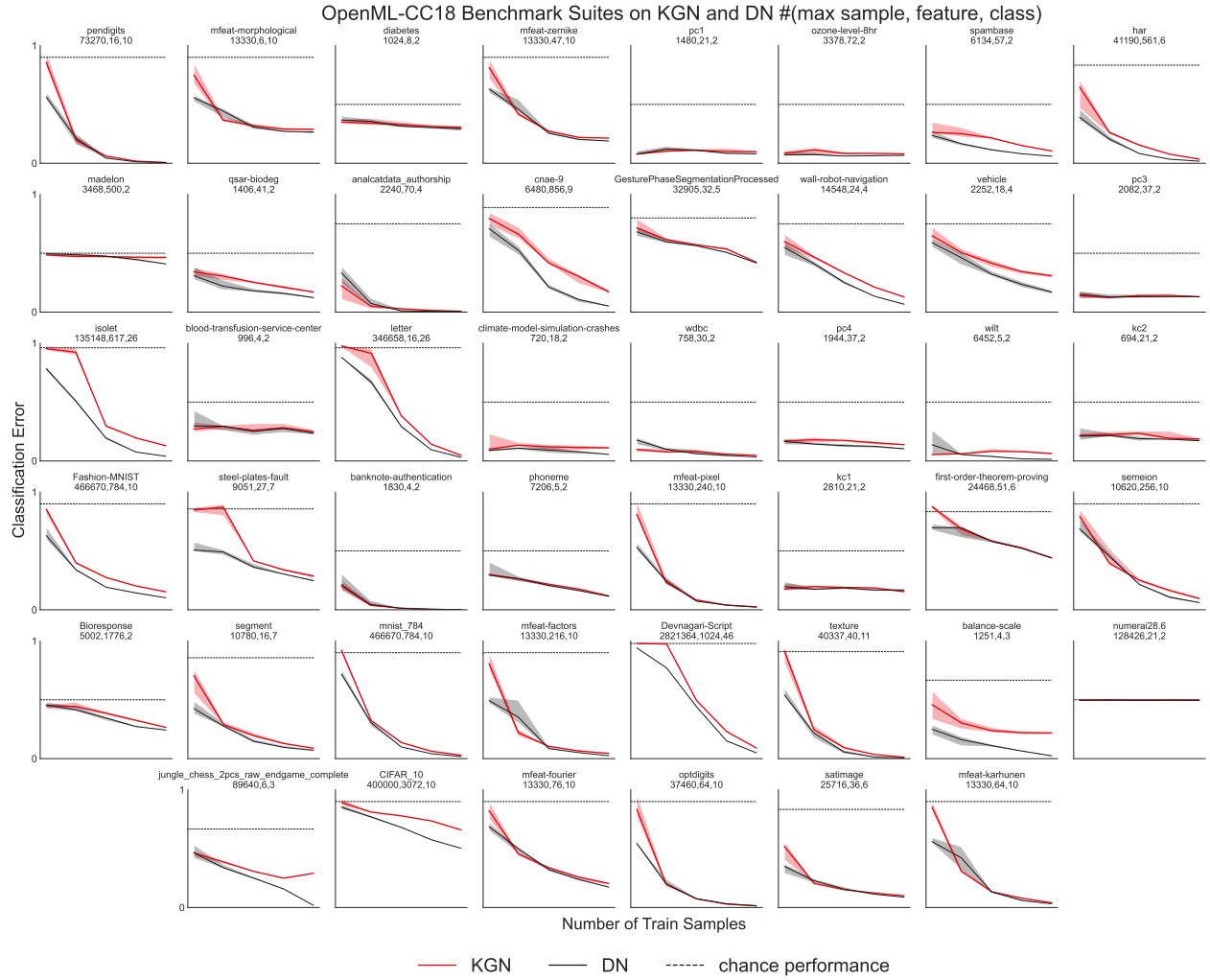


Figure 7: **Extended results on OpenML-CC18 datasets.** Classifications errors for KGN and REU-net with max sample size, number of features, and number of classes mentioned in the title for each panel.

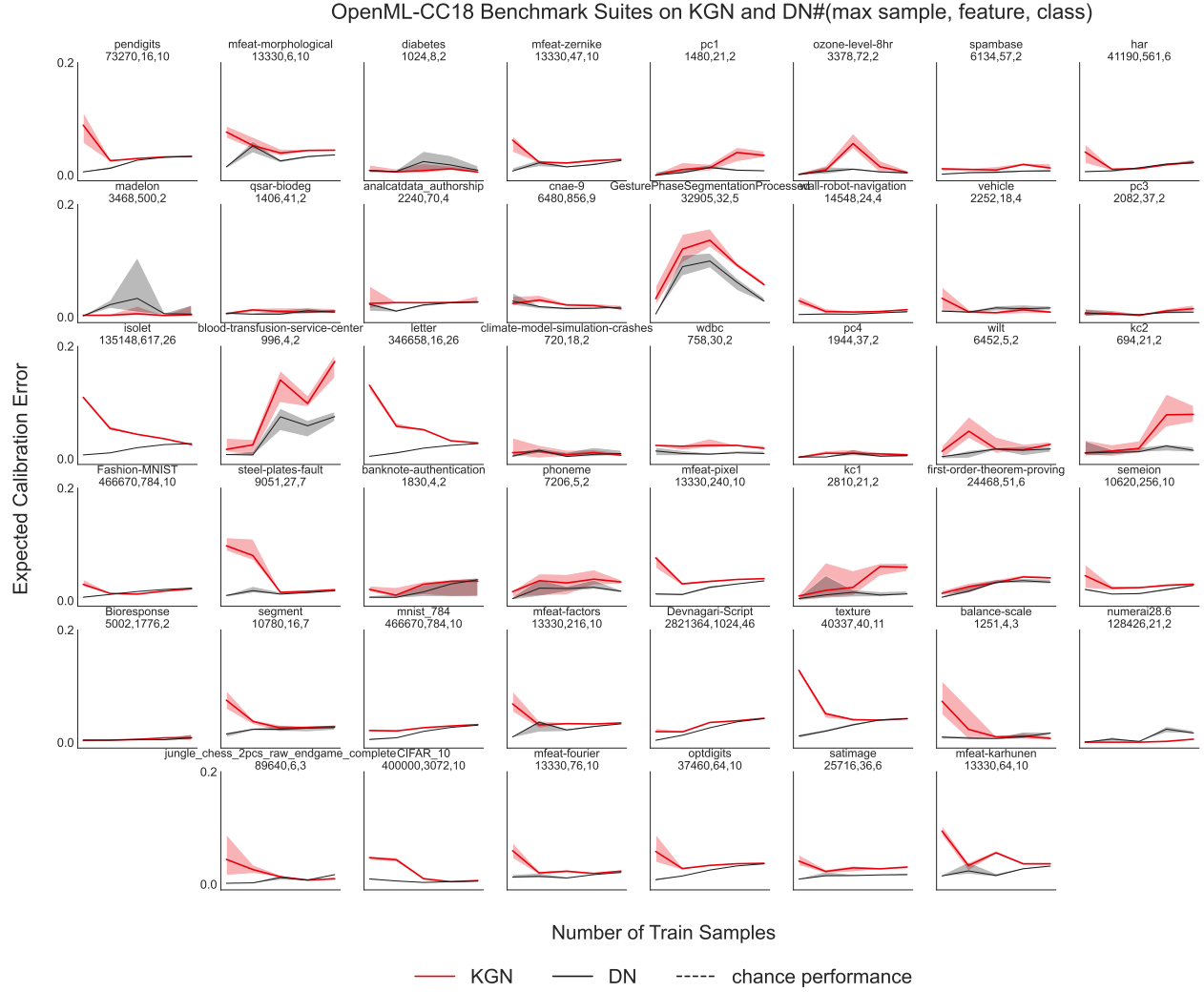


Figure 8: **Extended results on OpenML-CC18 datasets.** Calibration errors for KGN and R<sub>ELU</sub>-net with max sample size, number of features, and number of classes mentioned in the title for each panel.



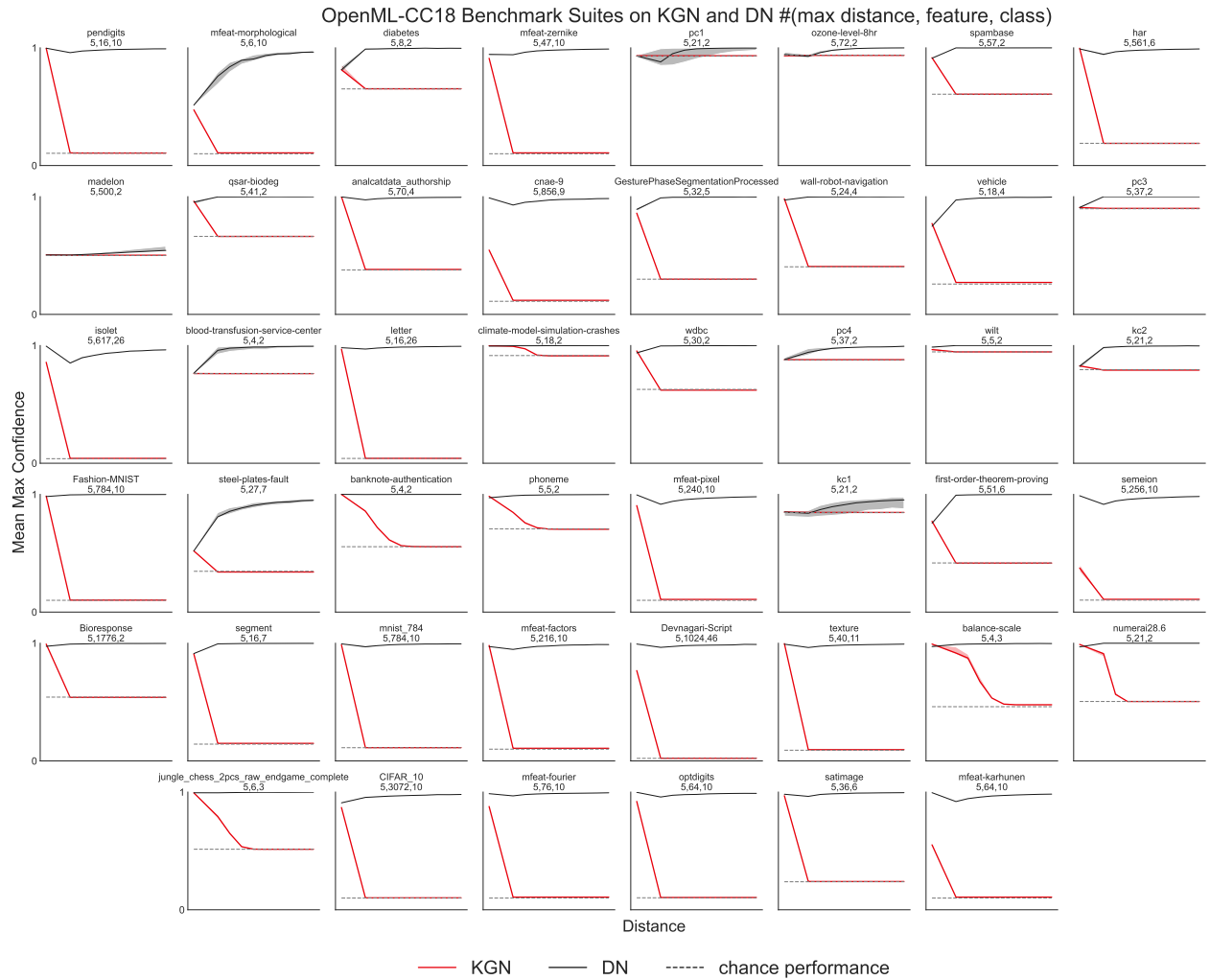


Figure 9: **Extended results on OpenML-CC18 datasets.** Mean max confidence for KGN and R<sub>E</sub>LU-net with max distance from the data origin, number of features, and number of classes mentioned in the title for each panel. The dashed line indicates the maximum of the empirical priors for different class labels.